Nucleon density of ^{172}Yb and ^{176}Yb at the nuclear periphery determined with antiprotonic x rays

R. Schmidt, F. J. Hartmann, and T. von Egidy
Physik-Department, Technische Universität München, D-85747 Garching, Germany

T. Czosnyka, J. Iwanicki, J. Jastrzębski, M. Kisieliński, P. Lubiński, P. Napiorkowski, L. Pieńkowski, and A. Trzcińska
Heavy Ion Laboratory, Warsaw University, Pl-02-097 Warsaw, Poland

J. Kulpa, R. Smolańczuk, and S. Wycech
Soltan Institute for Nuclear Studies, Pl-00-681 Warsaw, Poland

B. Kłos
Physics Department, Silesian University, Pl-40-007 Katowice, Poland

K. Gulda and W. Kurcewicz
Institute of Experimental Physics, Warsaw University, Pl-00-681 Warsaw, Poland

E. Widmann
CERN, CH-1211 Geneva 23, Switzerland

(Received 5 June 1998)

The antiprotonic x-ray cascade in ^{172}Yb and ^{176}Yb was studied and the widths and shifts of the levels which are affected by the strong interaction were deduced. A large number of transitions up to $\Delta n=5$ could be observed. This opened the possibility to determine for the first time also the widths of noncircular orbits. In ^{172}Yb and ^{176}Yb four level shifts and seven level widths were measured in each case. The widths are slightly increasing from ^{172}Yb to ^{176}Yb whereas the shifts stay roughly constant. The experimental intensities of the transitions are compared with results from calculations of the antiproton cascade. Using a Fermi distribution for the nucleon densities the neutron diffuseness parameter was deduced to be for ^{172}Yb (0.58 ± 0.04) fm larger than the proton diffuseness parameter. For ^{176}Yb this value is (0.71 ± 0.04) fm.
[S0556-2813(98)00712-2]

PACS number(s): 21.10.Gv, 13.75.Cs, 27.70.+q, 36.10.−k

I. INTRODUCTION

The proton distribution of a nucleus may be determined by several methods using the electromagnetic interaction between the protons and other charged particles. To investigate the neutron distribution this way is not open and one has to resort, e.g., to the strong interaction in hadronic atoms. Antiprotonic atoms are especially suited to probe the nuclear shape at large radii, as here the interaction with the nucleus takes place about 2 fm outside the half-density radius. In this nuclear region an enhanced neutron density was measured for a series of targets [1]. An especially high peripheral neutron density was found in ^{176}Yb.

Differences in the strong interaction of stopped antiprotons with different isotopes of the same element depend on the shape of the distribution of the nucleon density in the outer region of the nucleus, where the antiproton annihilation takes place, and should lead to differences in the widths and energy shifts of the lowest populated levels in antiprotonic atoms. Thus the comparison of neutron-deficient with neutron-rich isotopes should reveal an observable difference [2].

An experimental program aiming at the search of such an effect in a number of elements was conducted during the last two years of the operation of the Low Energy Antiproton Ring (LEAR) at CERN. In the present publication the results for ^{172}Yb and ^{176}Yb are given. The last transition of ^{174}Yb has already been measured at LEAR and the existence of a strong-interaction LS term was proposed [3].

II. PRINCIPLE OF THE MEASUREMENT

The principle of our experiments is simple: An incoming antiproton is finally slowed down in the target. After reaching an energy of some tens of eV it is captured by a target atom. In this process an electron with principal quantum number n_e is ejected, and the antiproton is captured into an antiprotonic-atom orbit with high principal quantum number $n_{\bar{p}}$: $n_{\bar{p}}\approx n_{e^-}\sqrt{m_{\bar{p}}/m_{e^-}}$ (cf. Ref. [4]). From this orbit it cascades down under emission of x rays and Auger electrons [5,6]. When the antiproton reaches states with low n the strong interaction becomes important and it annihilates. The strong interaction results in energy shifts and an increased level width of these states. Below these levels there is almost no antiproton population.

A combined analysis [7] correlates the observed strong interaction widths and shifts with the nucleon density at the nuclear periphery and the antiproton-nucleus optical potential. This analysis, which leads to information about the nuclear stratosphere, is based on the increased width of the

last observed transition due to strong interaction effects, the energy shift of the same transition compared to the pure electromagnetic energy, the increased width of the next to last populated level measured via the intensity balance between the transitions populating and depopulating this level, the absorption widths of higher levels determined via the intensity balance of these levels (due to the large number of transitions observed this could be done for the first time for ^{172}Yb and ^{176}Yb), and the neutron-to-proton density ratio and the absolute number of distant antiproton annihilations which lead to a cold residual nucleus. These two parameters could be determined for some cases, e.g., ^{176}Yb [1], with the method presented in [8]. Some of these observables were measured at LEAR for oxygen isotopes [2], ^{174}Yb and ^{138}Ba [3], and some lighter elements [9]. A compilation of pre-LEAR data can be found in Ref. [10].

In the present work we determined the antiprotonic cascade very comprehensively for transitions below $n=20$. Consequently, we were able to observe for the first time effects for all visible transitions sizably affected by the strong interaction. In ytterbium isotopes the corresponding antiprotonic levels are between $n=8$ and $n=11$.

Although more complicated potentials were recently introduced [11,12], frequently a simple optical potential model [13] is adequate for the calculation of the antiproton-nucleus interaction. If the strong interaction is treated as a perturbation to the electromagnetic solution of the Schrödinger equation the absorption width Γ and the shift ε of the energy levels are given by

$$\Gamma = 4\frac{\pi}{\mu_{\mathrm{N}\bar{\mathrm{p}}}}\mathrm{Im}(a_{\mathrm{N}\bar{\mathrm{p}}})\int \mathrm{d}R\,\rho(R)|\Psi_{\bar{\mathrm{p}}}(R)|^2 \qquad (1)$$

and

$$\varepsilon = 2\frac{\pi}{\mu_{\mathrm{N}\bar{\mathrm{p}}}}\mathrm{Re}(a_{\mathrm{N}\bar{\mathrm{p}}})\int \mathrm{d}R\,\rho(R)|\Psi_{\bar{\mathrm{p}}}(R)|^2 \qquad (2)$$

(N=p,n), where $\mu_{\mathrm{N}\bar{\mathrm{p}}}$ is the reduced mass of the antiproton-nucleon system, $a_{\mathrm{N}\bar{\mathrm{p}}}$ the scattering length of antiprotons on the proton or neutron, and $\Psi_{\bar{\mathrm{p}}}(R)$ the antiprotonic atom wave function (cf. Ref. [14]). These two formulas allow us to determine either the characteristics of the nucleon density $\rho(R)$ or the scattering length $a_{\mathrm{N}\bar{\mathrm{p}}}$. The value $a_{\mathrm{N}\bar{\mathrm{p}}}=(1.53+2.50i)$ fm was established with data taken before 1981 [10]. A more recent determination leads to $a_{\mathrm{N}\bar{\mathrm{p}}}=(2.4+3.4i)$ fm ([11], data set ISO). It is expected that $a_{\mathrm{N}\bar{\mathrm{p}}}$ is independent of the number of nucleons [11].

III. EXPERIMENTAL SETUP

The experiments were performed at the antiproton beam (momentum 414 MeV/c) provided by LEAR of CERN with a rather simple setup (cf. Fig. 1). The antiprotons were decelerated in a degrader; its thickness was adjusted to 51.5 mm polyethylene in order to stop a maximum number of antiprotons inside the target. A scintillation-counter telescope, consisting of an anticounter S_1 in front of the degrader and a counter S_2 (thickness 3 mm) behind it, identified the antiprotons. After passing the scintillator the antiprotons were stopped in the target. The targets of ^{172}Yb and ^{176}Yb had a thickness of 312 mg/cm^2 and 324 mg/cm^2, respectively.

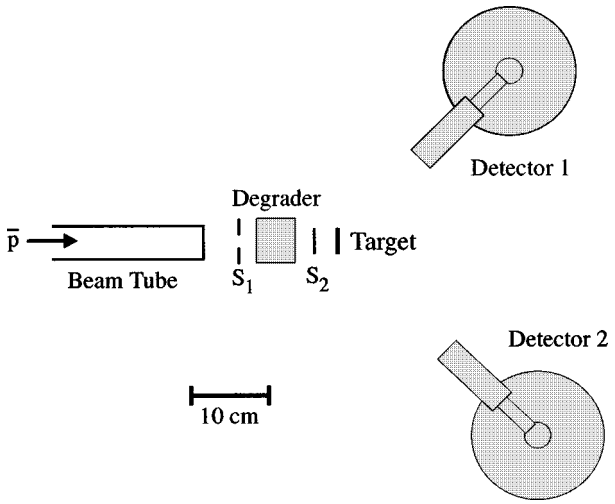

FIG. 1. Schematic view of the experimental setup: S_1, anticounter, and S_2, counter of the telescope.

The x rays emitted during the antiproton cascade were measured by two Ge detectors. Detector 1 was a planar HPGe detector with an active diameter of 25 mm and a sensitive depth of 13 mm, whereas detector 2 was a coaxial HPGe detector (relative efficiency 19%) with an outer diameter of 49 mm and a length of 49.5 mm. They were placed at distances of about 15 cm and 20 cm, respectively, from the target at angles of $\pm 45°$ towards the beam axis. The x rays were measured in coincidence with the antiproton signal in a time window which was extended up to 500 ns after the antiproton signal from the telescope counter.

In order to provide an on-line energy calibration, sources of ^{152}Eu and ^{192}Ir were placed close to the target and their γ-ray lines were measured during the whole data acquisition period. The calibration events, not coincident with antiprotons, were recorded with a prescaling factor of 21. Additionally pulser events were used to check the stability of the electronics. The energy calibration was found to be stable during the measurements. For a stability test the spectra were divided into 63 time intervals. The standard deviation from the mean value at 316.5 keV was found to be 89 eV. This allowed us to add all spectra taken during the measuring time of about 35 hours for each target.

Between the measurements the efficiencies of the Ge detectors were determined with sources positioned at the place of the target. Only relative efficiencies had to be measured for this experiment. In order to reach a sufficient number of counts in the last observable transition, spectra were collected for 1.1×10^9 antiprotons in the case of ^{172}Yb and for 1.5×10^9 antiprotons in the case of ^{176}Yb, identified with the counter telescope.

With a target thickness of about 300 mg/cm^2 the absorption of the x rays inside the target was large for small x-ray energies below about 150 keV. In order to increase the accuracy for transitions with low energies in a subsequent experiment a short measurement was done with an initial antiproton momentum of 100 MeV/c and targets with 115 mg/cm^2 thickness.

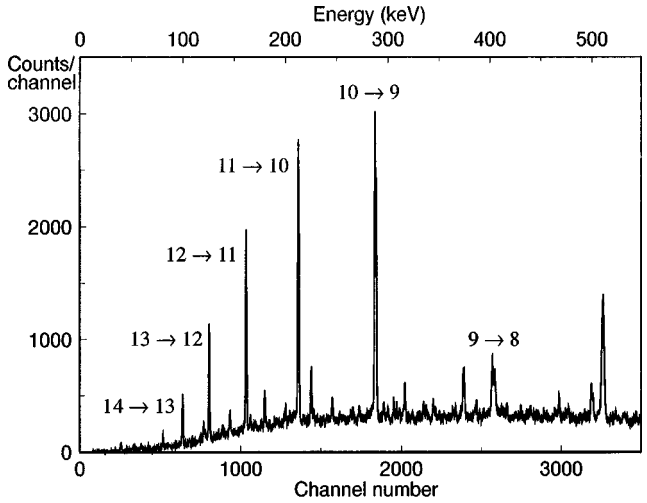

FIG. 2. Antiprotonic x-ray spectrum from ^{176}Yb measured with detector 2 (coaxial HPGe detector with an outer diameter of 49 mm and a length of 49.5 mm). One channel corresponds to 0.157 keV.

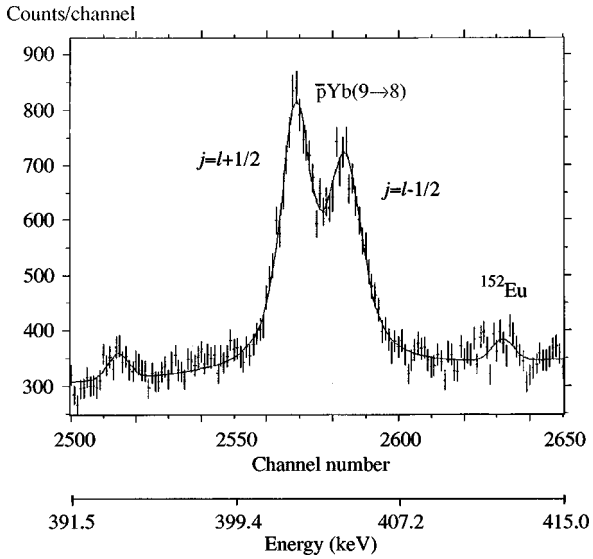

FIG. 3. Part of the x-ray spectrum from antiprotonic ^{176}Yb with the lines of the transition $n=9\rightarrow8$, measured with detector 2 (see also caption of Fig. 2).

IV. EXPERIMENTAL RESULTS

The accumulated x-ray spectrum from the ^{176}Yb target (thickness 324 mg/cm^2), as taken with detector 2, is shown in Fig. 2. Those lines in the spectra which are not broadened were fitted with Gaussians with width (FWHM) w. The energy dependence of w was fitted to these values by the function $w(E)=\sqrt{a+b\cdot E}$. For the peaks of the transition $n=9\rightarrow8$ a fit of two Lorentzians convoluted with Gaussians was employed. For the energy of this transition (403 keV) the FWHM of the Gaussian is $w=(1176\pm9)$ eV for detector 1 and $w=(1166\pm17)$ eV for detector 2.

The measured energy values are listed in Table I for the transitions $n=9\rightarrow8$ and $n=10\rightarrow9$. Figure 3 shows the part of the spectrum of ^{176}Yb of Fig. 2 in the energy region around the transitions $n=9\rightarrow8$. The fine structure of this line is clearly seen. The widths of the transitions $n=9\rightarrow8$ were derived from the Lorentzian widths of the doublet (cf. Table I).

The measured intensities of the antiprotonic x rays were corrected for the efficiencies of the detectors and the absorption of the x rays inside the target. The resulting relative intensities of the antiprotonic x rays from ^{172}Yb, normalized to the transition $n=12\rightarrow11$ for each target, are given in Fig. 4. Admixed transitions which contribute to the measured intensity are marked with an asterisk. The corresponding results for ^{176}Yb are presented in Fig. 5.

V. THE ANTIPROTON CASCADE

The intensities of the antiprotonic x rays from ^{172}Yb and ^{176}Yb were compared with results from cascade calculations based on a work by Leon [15]. In Leon's code the energies and widths of the lines influenced by strong interaction were determined by solving the Schrödinger equation for the sum of a Coulomb and a complex strong-interaction potential. For the scattering length $a_{\bar{N}p}$ the well established value $(1.53+2.50i)$ fm was used [10]. The nucleon density was assumed to be given by a two-parameter Fermi distribution

$$\rho_N(c_N,t_N,R)=\frac{\rho_{0N}}{1+e^{4\ln 3(R-c_N)/t_N}} \tag{3}$$

(N=p,n). Here R, c_N, t_N, and ρ_{0N} are the distance from the center of the nucleus, the half-density radius, the diffuseness parameter, and the normalization factor to the number of protons or neutrons of the nucleus, respectively. The rates for radiative dipole transitions were calculated from the formu-

TABLE I. Measured energies E and Lorentzian widths Γ of the transitions $n=(10\rightarrow9)$ and $n=(9\rightarrow8)$ and energy differences ΔE_m between the transitions.

Target	Transition $(n,j)\rightarrow(n',j')$	E(keV)	ΔE_m (keV)	Γ (keV)
^{172}Yb:	(10,19/2)→(9,17/2)	287.45±0.06	1.178±0.015	
	(10,17/2)→(9,15/2)	288.62±0.06		
	(9,17/2)→(8,15/2)	402.13±0.09	2.36±0.05	0.90±0.08
	(9,15/2)→(8,13/2)	404.48±0.09		1.18±0.10
^{176}Yb:	(10,19/2)→(9,17/2)	287.47±0.05	1.171±0.014	
	(10,17/2)→(9,15/2)	288.64±0.05		
	(9,17/2)→(8,15/2)	402.10±0.05	2.36±0.04	1.04±0.08
	(9,15/2)→(8,13/2)	404.46±0.06		1.29±0.10

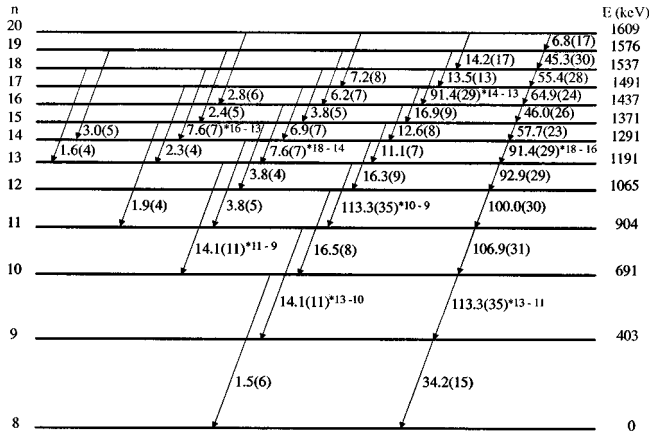

FIG. 4. Measured intensities of antiprotonic x-ray transitions in ^{172}Yb, normalized to the transition $n=12\rightarrow 11$; admixed transitions are marked with an asterisk. *E*: Level energy relative to the level $n=8$.

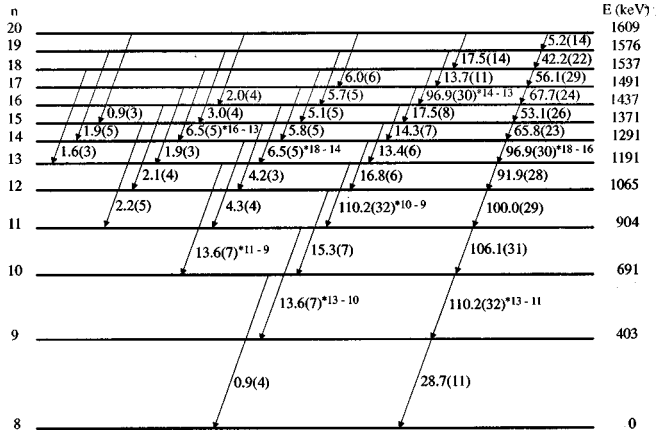

FIG. 5. Measured intensities of antiprotonic x-ray transitions in ^{176}Yb, normalized to the transition $n=12\rightarrow 11$; admixed transitions are marked with an asterisk. *E*: Level energy relative to the level $n=8$.

las given in Ref. [16]. The Auger rates were derived from the radiative rates and from cross sections for the photoeffect using Ferrell's formula [17]. Effects of electron depletion were neglected. This is a good approximation for metals as there the refilling rates for ejected electrons are high. The calculations started at $n=20$, where the antiproton is well inside the electron cloud. For transitions with $n>20$ the numerical stability of the code was not guaranteed. The initial antiprotonic l distribution at $n=20$ was assumed to be modified statistical with the population $N(l)\propto(2l+1)e^{\alpha l}$. Various other types of initial distributions were investigated, but this distribution led to the best agreement with the experiment. The parameters α of the initial distribution and the diffuseness t_n of the neutron density distribution were adjusted in order to get the best fit to the measured x-ray intensities for the transitions from levels with $n\leqslant 19$. For the proton parameters c_p and t_p of the Fermi distribution the data from Ref. [18], model a, were taken. In the more recent compilation [19] values for the proton distribution are given only for ^{176}Yb. In this reference two different values are presented, one of them being similar to Ref. [18].

The deformation of the nucleus was neglected. The difference c_n-c_p between the neutron and proton distribution was fixed at $c_n-c_p=0.13$ fm. This value was derived in Ref. [20] from HFB calculations for ^{208}Pb. It is almost the same for all neutron rich stable isotopes investigated and in agreement with results from inelastic α-particle scattering [21]. The parameters of the best fit are shown in Table II. The errors of α and t_n-t_p were derived from the variation of χ^2. The two free parameters α and t_n-t_p were found to be almost independent from each other.

With the large number of x-ray transitions fitted, it was possible to determine the difference t_n-t_p rather accurately. This offers a new method to determine the neutron density at the nuclear surface. While the initial l distribution is governed by the upper part of the cascade which is not influenced by strong-interaction effects, the nucleon density at the nuclear periphery is responsible for diminishing the intensities of the lower transitions depopulating levels with $n\leqslant 11$, which are affected by the strong interaction.

The measured intensities, normalized to the transition $n=12\rightarrow 11$, are compared in Fig. 6 for ^{176}Yb with values calculated using the parameters from Table II. The agreement is generally good. The intensities of the transitions depopulating the level $n=15$ of ^{172}Yb are by $(14\pm 5)\%$ smaller than those of ^{176}Yb. This may come from an E2 resonance which induces transitions from $n=15$ to $n=14$ of the antiprotonic atom by exciting the nucleus from the ground state 0^+ to the state 2^+ [22]. This effect is expected to be slightly larger in ^{172}Yb than in ^{176}Yb due to the larger quadrupole moment of the lighter isotope. This decrease in intensity is responsible for the higher χ^2 value of the fit, in which the E2 effect is not included, performed for ^{172}Yb, compared to that for ^{176}Yb (cf. Table II). Another explanation may come from an isotope effect in the opening of the K-Auger channel. It opens in antiprotonic Yb at $n\approx 16$ and has a large influence on the x-ray intensities.

The difference t_n-t_p increases from 0.58(4) fm for ^{172}Yb to 0.71(4) fm for ^{176}Yb. One should keep in mind that the method applied is sensitive only to a 2 fm to 3 fm wide region about 2 fm outside the half-density radius. The resulting density distribution outside this region is strongly model-dependent. With the parameters found for the proton and

TABLE II. Best-fit parameters of the cascade optimization. c_p, t_p, c_n, and t_n are the parameters of the two-parameter Fermi distribution for protons and neutrons, respectively, α is the parameter of the initial antiproton distribution for the cascade calculation, and f is used as defined in Eq. (4).

Target	c_p (fm)	t_p (fm)	(c_n-c_p) (fm)	(t_n-t_p) (fm)	α	χ^2	f
^{172}Yb	6.23	2.18	0.13	0.58 ± 0.04	0.098 ± 0.010	3.1	3.1
^{176}Yb	6.27	2.18	0.13	0.71 ± 0.04	0.092 ± 0.008	1.9	3.9

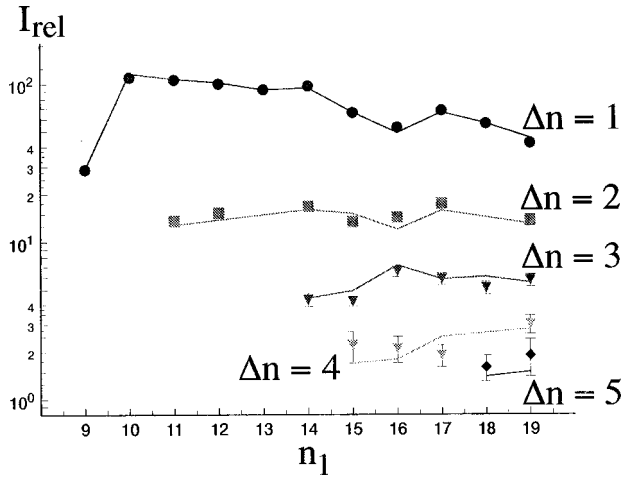

FIG. 6. Comparison of measured (points) and calculated (lines) relative intensities I_{rel} of the transitions $n=n_1\rightarrow n_1-\Delta n$ observed for antiprotonic ^{176}Yb. For the calculations the parameter set from Table II was used. All intensities were normalized to the intensity of the transition $n=12\rightarrow 11$.

neutron Fermi distributions the normalized value for the neutron-to-proton density ratio

$$f=\rho_{\mathrm{n}}(R)/\rho_{\mathrm{p}}(R)\cdot Z/N, \tag{4}$$

was folded with the antiproton absorption probability $A(R)$ (cf. Fig. 7). Its value came out to be $f=3.1$ for ^{172}Yb and $f=3.9$ for ^{176}Yb. In this region about 2 fm outside the nucleus where the antiproton annihilation takes place $\rho_{\mathrm{n}}(R)/\rho_{\mathrm{p}}(R)$ is strongly enhanced, compared to the value N/Z.

With the detection of residual nuclei after antiproton annihilation the neutron-to-proton density can be determined in

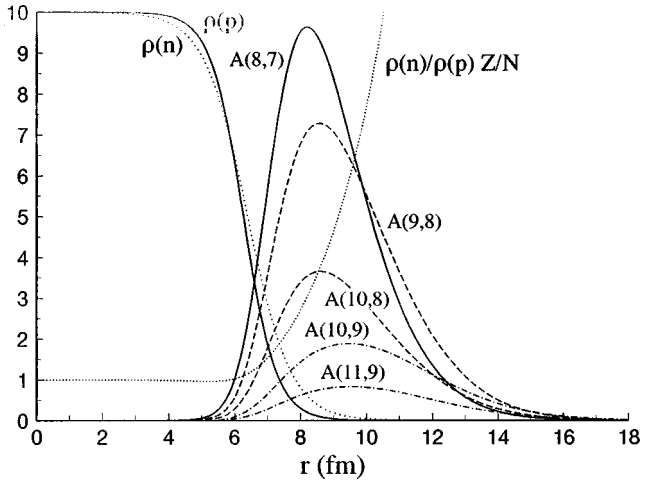

FIG. 7. Absorption probability $A(n,l)$ for antiprotons [level (8,7): solid line, (9,8) and (10,8): dashed lines, (10,9) and (11,9): dashed-dotted lines], proton (solid line) and neutron (dotted line) density, and neutron-to-proton density ratio (dotted line) for ^{176}Yb as a function of the distance from the nuclear center. The neutron and proton densities are normalized to ten in the center of the nucleus. The absorption probabilities are in arbitrary units. Those of (9,8) and (10,8) are magnified by a factor of 20 compared to that of (8,7), those of (10,9) and (11,9) by a factor of 400.

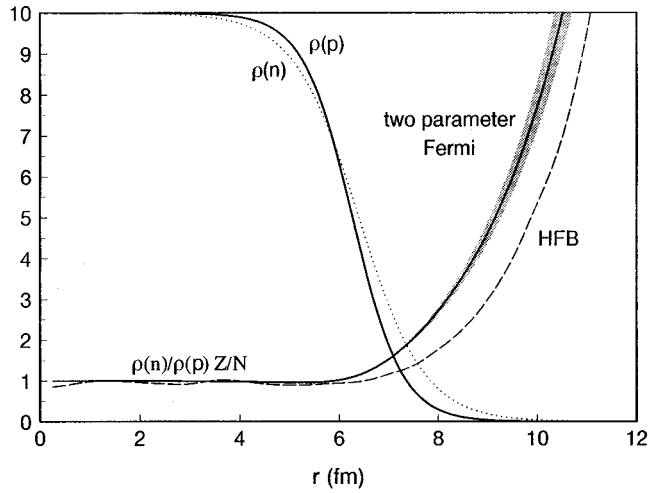

FIG. 8. Comparison of the neutron-to-proton density obtained for ^{176}Yb from this experiment (line) with results from HFB calculations (dashed line), displayed as a function of the distance to the nuclear center. The shadowed region corresponds to the error of $t_{\mathrm{n}}-t_{\mathrm{p}}=0.71\pm 0.04$ fm. The neutron and proton densities are normalized as in Fig. 7.

a more direct way. Such measurements provide, however, information on the nuclear surface in a region which is about 1 fm more peripheral than that from the measurement of antiprotonic x rays. The measured peripheral halo factor for ^{176}Yb from Ref. [1] is $f_{halo}^{periph}=8.4\pm 0.7$.

A comparison of the neutron-to-proton density ratio of the experimentally determined Fermi distribution for ^{176}Yb with that calculated from the Hartree-Fock-Bogoliubov model shows a larger experimental neutron density at the nuclear periphery (cf. Fig. 8).

VI. STRONG INTERACTION WIDTHS AND SHIFTS

In the previous section the nucleon density in the nuclear periphery was determined via the investigation of the antiprotonic cascade. Now observables are determined which are to be reproduced by models. This allows one to test different nucleon distributions and different values for the antiproton-nucleon interaction optical potential (cf. Sec. VII). The strong interaction widths of the different levels were deduced. Additionally strong interaction shifts could be measured for four levels. The measured shifts and widths of the transitions influenced by strong interaction are shown in Figs. 9 and 10 for ^{172}Yb and ^{176}Yb, respectively. The energy shifts given are the differences between the measured transition energies and those calculated with a purely electromagnetic potential. They reflect the real part of the complex scattering length $a_{\mathrm{N}\bar{\mathrm{p}}}$. For the calculation of the electromagnetic transition energies the Dirac equation was solved for the antiproton in the potential of an extended nucleus. Terms for the normal and anomalous magnetic moments of the antiproton were included as well as the vacuum polarization up to the seventh order and relativistic recoil corrections. These corrections lead to an accuracy of the binding energy of the antiprotonic level $(n,l)=(10,9)$ of lead of about 20 eV [23]. For the proton density a Fermi distribution with the parameters of Table II was used.

The experimental energies of antiprotonic x rays which

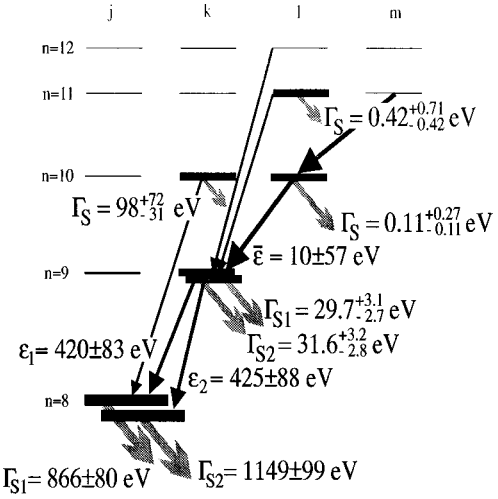

FIG. 9. Energy shifts of the transitions and widths for the levels of antiprotonic ^{172}Yb which are sizably influenced by the strong interaction. Γ_{S1} and ε_1: Widths and shift for $j=l+1/2$, Γ_{S2} and ε_2: Widths and shift for $j=l-1/2$. The widths of the levels (8,7) were derived from the widths of the transitions, those of the levels (9,8) and (10,9) from the intensity balance of these levels with small corrections for parallel transitions, and those of the levels (10,8) and (11,9) from the intensity balance with the feeding intensities taken from the adapted cascade.

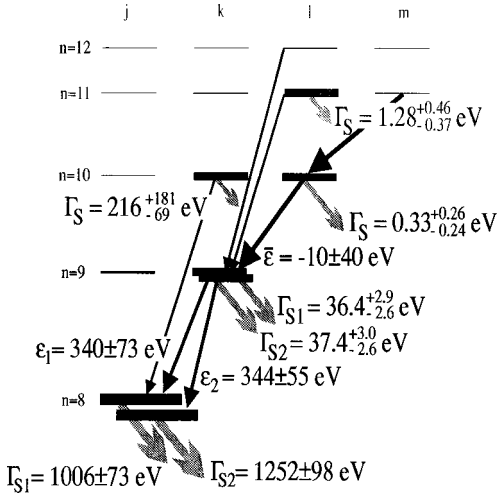

FIG. 10. The same as Fig. 9 for ^{176}Yb.

are not influenced by the strong interaction are in good agreement with the theoretical electromagnetic energies within their experimental errors. The binding energy of the last populated level $n=8$ was found to be increased by about 420 eV for ^{172}Yb and by about 340 eV for ^{176}Yb. In contrast to these attractive shifts repulsive shifts are expected from calculations [24]. The attractive shift comes from E2 coupling of the nuclear levels 0^+ and 2^+ with the atomic levels. The E2 shift was calculated for the transitions $(9\rightarrow 8)$ and $(10\rightarrow 9)$ using the method as described in Ref. [25]. Continuum effects were taken into account [26]. With these corrections the accuracy of the calculations is rather high. An uncertainty in the shift which may amount to several percent remains due to the uncertainty in the quadrupole moment with its large influence on the deduced E2 shifts. After correction the repulsive shift of the levels with $n=8$ is (205 ±83) eV and (200±46) eV for the $j=l+1/2$ states and (199±88) eV and (194±55) eV for the $j=l-1/2$ states in ^{172}Yb and ^{176}Yb, respectively. No significant differences are left between the corrected shifts of ^{172}Yb and ^{176}Yb (cf. Table III).

Without correction the energy of the transition $n=10\rightarrow 9$ is not shifted (cf. Figs. 9 and 10). With the E2 correction applied a mean repulsive strong-interaction shift of 133 eV results (cf. Table III).

The absorption widths of the levels with $(n,l)=(8,7)$ are slightly increasing from ^{172}Yb to ^{176}Yb. The width Γ_{S1} of the levels with $j=l+1/2$ is about 250 eV smaller than the width Γ_{S2} of the levels with $j=l-1/2$ (cf. Figs. 9 and 10). The widths of the $(n,l)=(9,8)$ levels were derived from the intensity balance of the transitions feeding and depopulating them. Transitions from higher levels and contributions of parallel transitions to the measured intensity were taken into account. For the transitions which were not observed the intensity values from the best-fit cascade calculations were taken. The correction is only about 2%. The population of the levels $(9,l)$, $l<8$ is very small, thus only antiprotons from the levels (9,8) are contributing to the intensity of the transition $(9\rightarrow 8)$. With the yield Y being the ratio of the

TABLE III. Measured energy shift ε_m of the transitions $n=(10,9)\rightarrow(9,8)$ and $n=(9,8)\rightarrow(8,7)$, correction ε_{E_2} due to the E2 coupling, and energy difference ΔE_m between the two main LS components of the transition $(9\rightarrow 8)$ compared to the calculated difference $\Delta E_{calc.}$; $\Delta E=\Delta E_m-\Delta E_{calc.}$. The values for ^{174}Yb are taken from Ref. [3].

Target	Transition $(n,j)\rightarrow(n',j')$	ε_m (eV)	ε_{E_2} (eV)	$(\varepsilon_m-\varepsilon_{E_2})$ (eV)	ΔE (eV)
^{172}Yb:	(10,19/2)→(9,17/2)	6±59	143	−137±59	7±15
	(10,17/2)→(9,15/2)	13±59	143	−130±59	
	(9,17/2)→(8,15/2)	420±83	625	−205±83	6±48
	(9,15/2)→(8,13/2)	425±88	624	−199±88	
^{174}Yb:	(9,17/2)→(8,15/2)	283±36 [3]	633	−350±36	58±26 [3]
	(9,15/2)→(8,13/2)	341±43 [3]	631	−290±43	
^{176}Yb:	(10,19/2)→(9,17/2)	−8±44	123	−131±44	−5±14
	(10,17/2)→(9,15/2)	−13±44	123	−136±44	
	(9,17/2)→(8,15/2)	340±46	540	−200±46	6±38
	(9,15/2)→(8,13/2)	344±55	538	−194±55	

TABLE IV. Radiation width Γ_{em} and Auger width Γ_{Auger} for those levels where the strong interaction width was determined via the intensity balance.

	^{172}Yb		^{176}Yb	
(n,l)	Γ_{em} (eV)	Γ_{Auger} (eV)	Γ_{em} (eV)	Γ_{Auger} (eV)
(9,8)	11.63	0.09	11.48	0.08
(10,8)	8.50	0.10	8.39	0.10
(10,9)	6.77	0.12	6.69	0.12
(11,9)	5.10	0.14	5.04	0.14

intensities of the transitions depopulating the level to the intensities of the transitions populating it, the width Γ_S of the level due to the strong interaction is [27]

$$\Gamma_S = \Gamma_{em}\left(\frac{1}{Y} - 1\right) - \Gamma_{Auger}. \quad (5)$$

Here Γ_{em} and Γ_{Auger} are the radiation and Auger widths, respectively, of the levels with observable strong interaction widths. They are summarized in Table IV. Significant differences in the strong interaction widths of the levels (9,8) were found between ^{172}Yb and ^{176}Yb: the mean widths of the level (9,8) are $\Gamma_S = 30.6^{+2.4}_{-2.2}$ eV and $\Gamma_S = 36.9^{+2.5}_{-2.2}$ eV for ^{172}Yb and ^{176}Yb, respectively. The width of the level (10,9) was determined in the same way from the intensity balance of this level. While this width is still compatible with zero for ^{172}Yb, in ^{176}Yb already some absorption occurs from this level.

In previous experiments only widths for one or two circular transitions were determined for each nucleus. Due to the high number of transition intensities measured for ^{172}Yb and ^{176}Yb the antiprotonic cascade could be determined rather accurately in this experiment. In order to deduce the yield of the levels (10,8) and (11,9), the intensities of the transitions feeding those levels were derived from these cascade calculations which had been adapted to the measured intensities. These intensities depend only weakly on the strength of the antiproton-nucleus strong interaction, as the upper part of the cascade is almost independent of the nuclear density distribution. If the strong interaction is neglected, the calculated intensities of the lines feeding the level change by only 5% for (10,8) and by only 2% for (11,9). For the level with $(n,l) = (11,9)$ again only for ^{176}Yb a sizable effect of the strong interaction shows up. From the level (10,8) antiprotons are strongly absorbed. The intensity of the transition $10 \rightarrow 8$ is diminished by factors of about six and ten in antiprotonic ^{172}Yb and ^{176}Yb, respectively, compared to the cascade calculated without strong absorption.

Figure 11 shows an overview over the widths and shifts of the transition $(9 \rightarrow 8)$ in antiprotonic ^{172}Yb and antiprotonic ^{176}Yb and the corresponding ^{174}Yb data previously measured [3], corrected for the E2 shift. Due to the higher statistics the errors of the data from Ref. [3] are smaller than those from the present experiment. From ^{172}Yb to ^{176}Yb the width is slightly increasing, whereas the shift stays roughly constant.

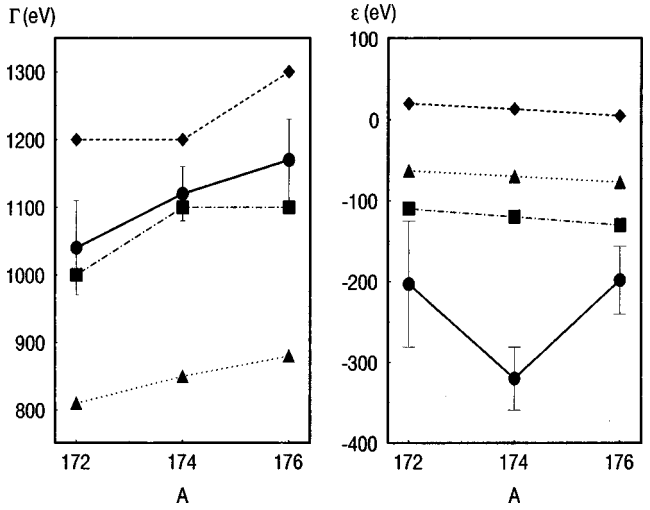

FIG. 11. Widths and shifts of the transition $n = 9 \rightarrow 8$ for the even Yb isotopes from ^{172}Yb to ^{176}Yb (full circles). The data of ^{174}Yb are taken from Ref. [3]. The shifts are corrected for the E2 effect. The triangles, squares, and diamonds show the results of calculations with nuclear densities based on HFB calculations with different optical potentials and folding root-mean-square radii (models A, B, and C, respectively; cf. Table V).

VII. CALCULATED WIDTHS AND SHIFTS

The shifts and widths listed in Table V have been calculated with nuclear densities based on the Hartree-Fock-Bogoliubov model with Skyrme III forces used in Ref. [14]. The nucleus was assumed to be spherical. To obtain the antiproton optical potentials these densities were folded with Gaussian form factors to account for the antiproton-nucleon interaction range. The strength parameters of these models as expressed by phenomenological effective lengths are: $a_{N\bar{p}} = (1.53 + 2.5i)$ fm (model A and C) and $a_{N\bar{p}} = (2.4 + 3.4i)$ fm (model B). A folding root-mean-square range $r = 0.8$ fm was taken for the models A and B. This range corresponds to the charge density profile used in the early optical-potential fit of Ref. [10] (model A) and in the recent fit to $\bar{p}$ atomic data (Ref. [11], data set ISO) (model B).

An inspection of Table V shows that model B agrees fairly well with the measured strong interaction width of the level (8,7), while model A is not compatible at all. The widths of higher levels and the level shifts are not reproduced by any of these models. It is, however, not the aim of this publication to determine a better estimate of the optical potential parameters, since this simple form of the potential is not satisfactory in this case. There are two reasons:

In our measurements the nuclear effects are determined predominantly by the neutron density. This density is rather uncertain in the region about 2 fm outside the half-density radius, where the interaction takes place. It is the purpose of the present investigation to provide new information on neutron densities at the nuclear periphery. Figure 8 shows that the HFB model underestimates the neutron density in this region for ^{176}Yb. This may explain the differences in the upper widths of this nucleus between experiment and theory. For a complete analysis more nuclei should be studied.

The Yb nuclei are strongly deformed. In such a case the optical potential calculated by a simple angular average over the deformed-nucleus density is not precise enough. This

TABLE V. Shifts $\varepsilon_{(n,l)\to(n',l')}$ of the transitions and widths $\Gamma_{(n,l)}$ of the levels from Hartree-Fock-Bogoliubov calculations of the nuclear density averaged over the fine structure components [model A: $a=(1.53+2.5i)$ fm, $r=0.8$ fm; model B: $a=(2.4+3.4i)$ fm, $r=0.8$ fm; model C: $a=(1.53+2.5i)$ fm, $r=1.5$ fm], compared with the experimental values.

Target:	^{172}Yb				^{176}Yb			
Model:	A	B	C	Exp.	A	B	C	Exp.
$\Gamma_{(8,7)}$ (keV)	0.81	1.0	1.2	1.04 ± 0.07	0.88	1.1	1.3	1.17 ± 0.06
$\varepsilon_{(9,8)\to(8,7)}$ (eV)	-63	-110	20	-203 ± 78	-77	-130	4.7	-198 ± 42
$\Gamma_{(9,8)}$ (eV)	15	20	22	$30.6^{+2.4}_{-2.2}$	16	22	25	$36.9^{+2.5}_{-2.2}$
$\varepsilon_{(10,9)\to(9,8)}$ (eV)	0.58	0.57	4.1	-133 ± 57	0.58	0.55	4.2	-133 ± 40
$\Gamma_{(10,9)}$ (eV)	0.17	0.23	0.24	$0.11^{+0.27}_{-0.11}$	0.19	0.27	0.28	$0.33^{+0.26}_{-0.24}$
$\Gamma_{(10,8)}$ (eV)	43	57	54	98^{+72}_{-31}	50	64	59	216^{+181}_{-69}
$\Gamma_{(11,9)}$ (eV)	0.50	0.70	0.74	$0.42^{+0.71}_{-0.42}$	0.58	0.80	0.84	$1.28^{+0.46}_{-0.37}$

Target:	^{174}Yb			
Model:	A	B	C	Exp. (from Ref. [3], corrected for E2 shift)
$\Gamma_{(8,7)}$ (keV)	0.85	1.1	1.2	1.12 ± 0.04
$\varepsilon_{(9,8)\to(8,7)}$ (eV)	-70	-120	13	-320 ± 39

happens because of the strong p-wave antiproton-nucleus interaction which is induced by density gradients. In addition to the well known radial gradient also some tangential contributions arise. These require a subtle analysis: similar effects of the tangential density gradient were found to yield a 20% correction to the nuclear LS interactions [28]. A theoretical analysis of these effects is in preparation.

Nevertheless, to learn about the significance of several optical potential parameters, some tests have been performed. Ways to increase the absorption predicted by model A are to enhance the attraction or to extend its range. There are good reasons to have the real part of the optical potential extended sizeably over the nuclear density. This may be due to the long-range pion exchange potential affecting the $N-\bar{p}$ scattering matrix to second and higher orders. An attractive tail is expected from theory and is also found in the description of the low energy antiproton-nucleus scattering [29], where a folding range as high as $r=1.5$ fm was used for the real part of the potential. This folding range was taken for model C. It produces absorption widths which are close to those from model B, but fails even more for the level shifts.

The shifts of the levels offer more challenges to the determination of $a_{\mathrm{N}\bar{\mathrm{p}}}$ and the nucleon density distribution. The calculated strong-interaction shifts are for all models much smaller than the measured ones. For the transition $(9\to8)$ the shift of model B has at least the same order of magnitude as the measured shift. The shift of the transition $(10\to9)$, however, cannot be explained with the different models. As mentioned before this repulsive shift of about 130 eV arises after the correction due to the E2 effect of the quadrupole moment of the nucleus (cf. Table III). It is about 50% of the shift of the transition $(9\to8)$ whereas the expected strong-interaction shift is less than 5 eV. Octupole excitations of the nucleus were considered, but their influence on the shifts is negligible. It has to be stated that there remains a serious discrepancy between experimental and theoretical strong-interaction shifts. If the E2 shift is applied the calculated strong-interaction shift of the transition $(9\to8)$ roughly agrees with the experiment and the calculation fails for the transition $(10\to9)$, if the E2 shift is not taken into account theory fails for the transition $(9\to8)$ but the shift of the transition $(10\to9)$ is reproduced.

The LS splitting observed in this experiment is essentially due to the electromagnetic fine structure. Additionally, interactions of the antiproton with the nucleus may affect this splitting and broaden the levels in a different way. The main part of this effect is purely geometrical and comes from the difference in the radii of the orbits of the two fine structure states. This difference arises since the electromagnetic LS potential is attractive in the lower state but repulsive in the upper one. Hence, the overlap of the atomic wave function with the nucleus is larger in the lower component. In consequence this state has larger width Γ_{S2} and shift ε_2. Numerically one finds that the ratio

$$R(n):=\frac{\Gamma_{\mathrm{S2}}-\Gamma_{\mathrm{S1}}}{(\Gamma_{\mathrm{S2}}+\Gamma_{\mathrm{S1}})/2} \tag{6}$$

is fairly independent of the optical potential. For ^{176}Yb it is $R(8)=0.085$ in the case of potential A and thus the difference in the widths due to the different geometries of the two LS states is 0.096 keV. This difference constitutes almost half of the observed difference of (0.25 ± 0.12) keV (cf. Fig. 10). The rest of the experimental difference of about 0.15 keV is to be attributed to the nuclear LS interactions. For the level $n=9$ one finds $R(9)=0.068$ and the geometric difference of the widths is 2.5 eV, which agrees with the experiment. The overlap effect also repulses the wave function of the lower fine structure state of the level $n=8$ more than that of the upper state. The calculated energy difference is 17 eV for model A. The shift of the two states with $n=8$, $j=15/2$, and $j=13/2$ has the same value within the errors (cf. Table III). The small difference which is expected is obscured by the experimental errors.

The difference in the widths of the level $n=8$ in ^{172}Yb and ^{176}Yb is in agreement with the results of Ref. [3], where an LS-effect was searched for in ^{174}Yb. However, the ^{174}Yb data did not confirm the theoretical expectation of a more

repulsive shift for the lower component of the level $n=8$. The observed value of ΔE (cf. Table III) has the opposite sign than that which was expected from theory [3].

VIII. SUMMARY

The antiprotonic cascade of ^{172}Yb and ^{176}Yb was investigated. With the widths and shifts measured for the antiprotonic levels with principal quantum numbers from $n=8$ to $n=11$ eleven observables were determined which may be used for a combined analysis of the nuclear surface and the antiproton-nucleus interaction. Differences were found between ^{172}Yb and ^{176}Yb which show the nucleon density to increase with A in the region about 2 fm outside the half-density radius. Three different methods were used to derive the level widths. The widths of the levels (8,7) were taken directly from the line widths of the transitions, those of the levels (9,8) and (10,9) from the intensity balance for these levels with small corrections for parallel transitions, and those of the levels (10,8) and (11,9) from the intensity balance with the feeding intensities taken from the best-fit cascade calculations.

Applying a Fermi distribution for the nucleon density the measured antiprotonic x-ray intensities may be well reproduced. With $c_n - c_p$ taken as 0.13 fm, the neutron diffuseness parameter was deduced to be larger than the proton diffuseness parameter by (0.58 ± 0.04) fm for ^{172}Yb and (0.71 ± 0.04) fm for ^{176}Yb. The ratio of the neutron-to-proton density in the region where the annihilation takes place is shown to be enhanced, compared to the value inside the nucleus, by factors of about three and four for ^{172}Yb and ^{176}Yb, respectively. The neutron-to-proton density deduced is in agreement with the peripheral halo factor [1].

Using different values for the strength of the antiproton-nucleus potential and different neutron-density distributions one finds a number of ways to reproduce the experimental level widths by calculations, but the level shifts could not be explained. If the E2 correction is applied, all models used give calculated shifts for the level $n=9$ which are smaller than the measured ones. Without correction, however, the shift of the level $n=8$ cannot be described at all. A small LS-splitting effect has been observed.

ACKNOWLEDGMENTS

We thank the LEAR team for providing the intense, high-quality antiproton beam and Anna Stolarz from the Heavy Ion Laboratory in Warsaw and Katharina Nacke and Peter Maier-Komor of the Technical University Munich for the target preparation. Financial support by the Accelerator Laboratory of the University and the Technical University of Munich as well as by the Polish State Committee for Scientific Research under the Grant No. 2 P03B 048 15 is acknowledged. This work was supported by the Volkswagen Foundation.

[1] P. Lubiński, J. Jastrzębski, A. Grochulska, A. Stolarz, A. Trzcińska, W. Kurcewicz, F. J. Hartmann, W. Schmid, T. von Egidy, J. Skalski, R. Smolańczuk, S. Wycech, D. Hilscher, D. Polster, and H. Rossner, Phys. Rev. Lett. **73**, 3199 (1994).

[2] Th. Köhler, P. Blüm, G. Büche, A. D. Hancock, H. Koch, A. Kreissl, H. Poth, U. Raich, D. Rohmann, G. Backenstoss, Ch. Findeisen, J. Repond, L. Tauscher, A. Nilsson, S. Carius, M. Suffert, S. Charalambus, M. Chardalas, S. Dedoussis, H. Daniel, T. von Egidy, F. J. Hartmann, W. Kanert, G. Schmidt, J. J. Reidy, M. Nicholas, and A. Wolf, Phys. Lett. B **176**, 327 (1986).

[3] A. Kreissl, A. D. Hancock, H. Koch, Th. Köhler, H. Poth, U. Raich, D. Rohmann, A. Wolf, L. Tauscher, A. Nilsson, M. Suffert, M. Chardalas, S. Dedoussis, H. Daniel, T. von Egidy, F. J. Hartmann, W. Kanert, H. Plendl, G. Schmidt, and J. J. Reidy, Z. Phys. A **329**, 235 (1988).

[4] G. A. Baker, Phys. Rev. **117**, 1130 (1960).

[5] E. Fermi and E. Teller, Phys. Rev. **72**, 399 (1947).

[6] M. Leon and R. Seki, Nucl. Phys. **A282**, 445 (1977).

[7] C. J. Batty, E. Friedman, H. J. Gils, and H. Rebel, Adv. Nucl. Phys. **19**, 1 (1989).

[8] J. Jastrzębski, H. Daniel, T. von Egidy, A. Grabowska, Y. S. Kim, W. Kurcewicz, P. Lubiński, G. Riepe, W. Schmid, A. Stolarz, and S. Wycech, Nucl. Phys. **A558**, 405c (1993).

[9] H. Poth, H. Barth, G. Büche, A. D. Hancock, H. Koch, Th. Köhler, A. Kreissl, U. Raich, D. Rohmann, A. Wolf, L. Tauscher, A. Nilsson, M. Suffert, M. Chardalas, S. Dedoussis, H. Daniel, T. von Egidy, F. J. Hartmann, W. Kanert, H. S. Plendl, G. Schmidt, and J. J. Reidy, Nucl. Phys. **A466**, 667 (1987).

[10] C. J. Batty, Nucl. Phys. **A372**, 433 (1981).

[11] C. J. Batty, E. Friedman, and A. Gal, Nucl. Phys. **A592**, 487 (1995).

[12] C. J. Batty, E. Friedman, and A. Gal, Phys. Rep. **287**, 385 (1997).

[13] S. Wycech, F. J. Hartmann, H. Daniel, W. Kanert, H. S. Plendl, T. von Egidy, J. J. Reidy, M. Nicholas, L. A. Redmond, H. Koch, A. Kreissl, H. Poth, and D. Rohmann, Nucl. Phys. **A561**, 607 (1993).

[14] S. Wycech, J. Skalski, R. Smolańczuk, J. Dobaczewski, and J. R. Rook, Phys. Rev. C **54**, 1832 (1996).

[15] M. Leon and R. Seki, Phys. Rev. Lett. **32**, 132 (1974).

[16] Y. Eisenberg and D. Kessler, Nuovo Cimento **19**, 1195 (1961).

[17] R. A. Ferrell, Phys. Rev. Lett. **4**, 425 (1960).

[18] R. Engfer, H. Schneuwly, J. L. Vuilleumier, H. K. Walter, and A. Zehnder, At. Data Nucl. Data Tables **14**, 509 (1974).

[19] H. de Vries, C. W. de Jager, and C. de Vries, At. Data Nucl. Data Tables **36**, 495 (1987).

[20] J. Dechargé and D. Gogny, Phys. Rev. C **21**, 1568 (1980).

[21] A. Krasznahorkay, J. Bacelar, J. A. Bordewijk, S. Brandenburg, A. Buda, G. van 't Hof, M. A. Hofstee, S. Kato, T. D. Poelhekken, S. Y. van der Werf, A. van der Woude, M. N. Harakeh, and N. Kalantar-Nayestanaki, Phys. Rev. Lett. **66**, 1287 (1991).

[22] B. A. Jacobsohn, Phys. Rev. **96**, 1637 (1954).

[23] E. Borie, Phys. Rev. A **28**, 555 (1983).

[24] C. J. Batty, in *Antiproton-Nucleon and Antiproton-Nucleus Interactions*, edited by F. Bradamante *et al.* (Plenum Press, New York, 1990), p. 251.
[25] A. M. Green, G. Q. Liu, and S. Wycech, Nucl. Phys. **A483**, 619 (1988).
[26] G. Q. Liu, A. M. Green, and S. Wycech, Nucl. Phys. **A495**, 622 (1989).
[27] H. Koch, G. Poelz, H. Schmitt, L. Tauscher, G. Backenstoss, S. Charalambus, and H. Daniel, Phys. Lett. **28B**, 279 (1968).
[28] S. Wycech, H. Poth, and J. R. Rook, Z. Phys. A **335**, 355 (1990).
[29] E. Friedman and J. Lichtenstadt, Nucl. Phys. **A455**, 573 (1986).